# Electronic Supplementary Information

## MCM-41 support to ultrasmall $\gamma$-$Fe_2O_3$ nanoparticles for $H_2S$ removal

C. Cara,[abc] E. Rombi,[a] A. Musinu,[ac] V. Mameli,[ac] A. Ardu,[abc] M. Sanna Angotzi,[ac] L. Atzori[a], D. Niznansky,[d,e] H. L. Xin[f] and C. Cannas*[abc]

[a]Department of Chemical and Geological Sciences, Università di Cagliari, S.S. 554 bivio per Sestu, 09042, Monserrato (CA), Italy

[b]Consorzio AUSI, Palazzo Bellavista Monteponi, 09016 Iglesias, CI, Italy

[c]INSTM, Cagliari Unit

[d]Department of Inorganic Chemistry, Charles University of Prague, Prague 116 36, Czech Republic

[e]AS CR, Inst. Inorgan. Chem., vvi, Husinec Rez 25068, Czech Republic

[f]Center for Functional Nanomaterials, Brookhaven National Laboratory, Upton, New York, United States

*Address correspondence to Carla Cannas: ccannas@unica.it

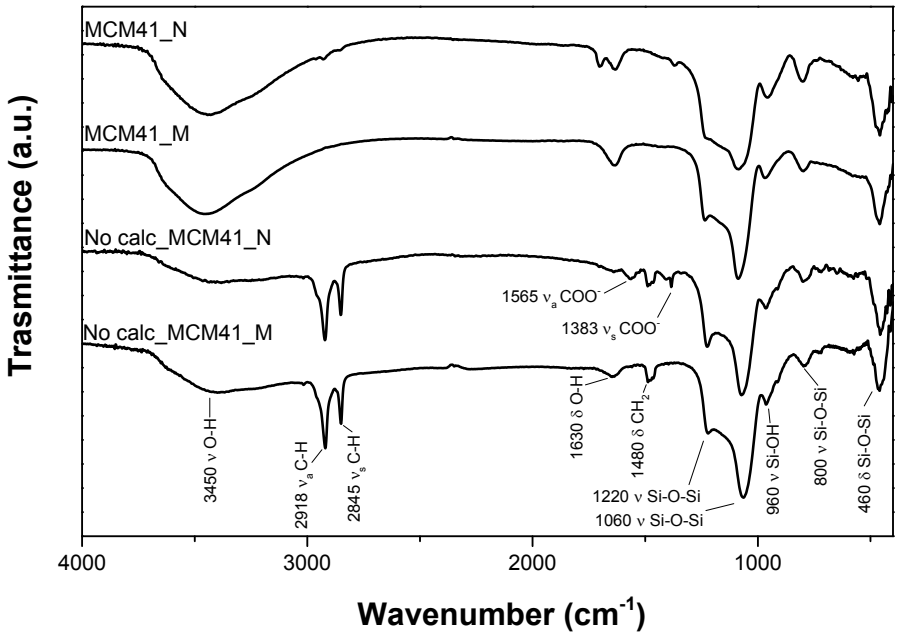


**Figure 1S:** FTIR spectra of samples before (No calc_MCM41_M and No calc_MCM41_N) and after calcination (MCM41_M and MCM41_N).

Figure 1S reports FTIR spectra of the supports before and after calcination. Both samples before calcination exhibit different vibrational modes attributable to the presence of CTAB: asymmetric and symmetric C-H stretching (2918 $cm^{-1}$ and 2845 $cm^{-1}$), bending (1450 $cm^{-1}$), and rocking (1400-720 $cm^{-1}$) modes of $CH_2$ group. Two additional peaks at 1585 $cm^{-1}$ and 1383 $cm^{-1}$ are present in MCM41_N sample synthesized using ethyl acetate as a growth inhibitor agent of the particles. These peaks should be attributed to asymmetric and symmetric $COO^-$ stretching modes due to the formation of acetate formed by the hydrolysis of ethyl acetate.

**Table 1S:** Two-Solvents impregnation conditions and %w/w of iron oxide in each sorbent.

| Sample | Pore volume ($cm^3g^{-1}$) | Amount of aqueous solution (μL) | Concentration of $Fe(NO_3)_3 \cdot 9H_2O$ solution | Real Amount of $Fe_2O_3$ (% w/w) |
|---|---|---|---|---|
| MCM41_M | 0.76 | 83 | 1.5 | 9.6 |
| MCM41_N | 0.80 | 98 | 1.3 | 9.6 |
| SBA15 | 1.10 | 125 | 1.1 | 10.0 |

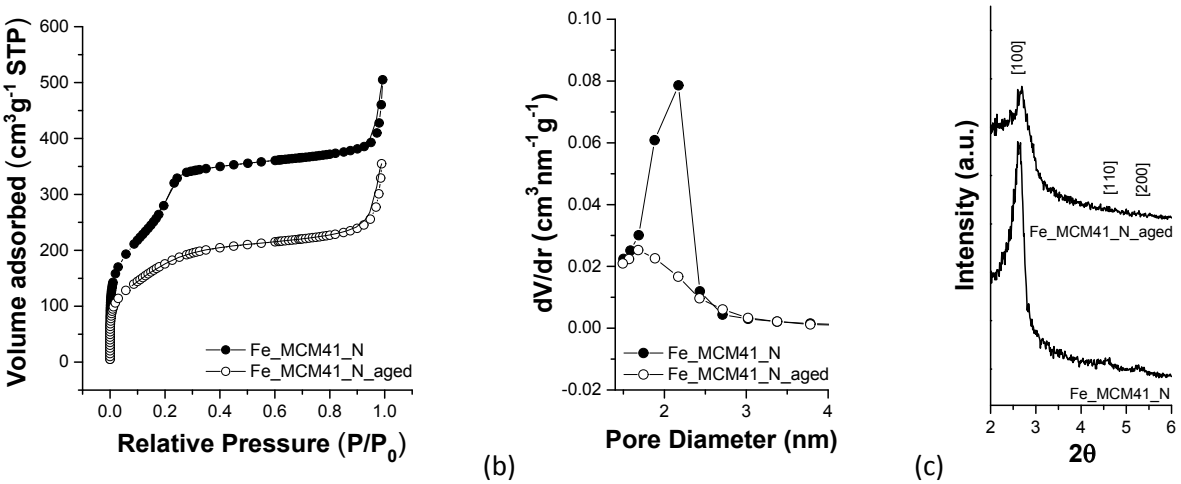


(a) (b) (c)

**Figure 2S:** $N_2$ adsorption- desorption isotherm (a), pore size distribution (b) and Low angle (c) of Fe_MCM41_N and Fe_MCM41_N_aged.

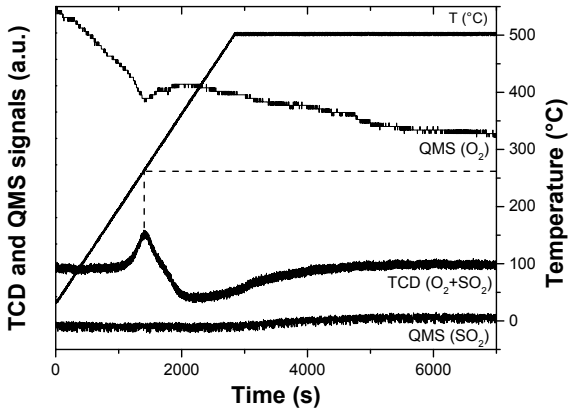


(a)

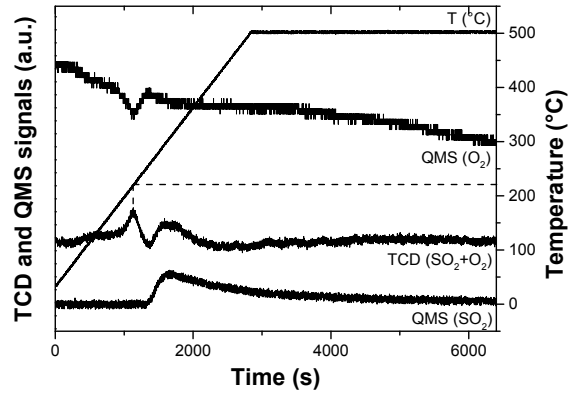


(b)

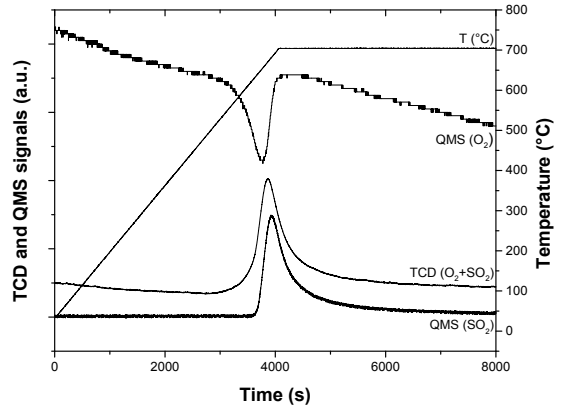


(c)

**Figure 3S:** TPD profile and $SO_2$ and $O_2$ Quadrupole Mass Spectrometer (QMS) signals of Fe_MCM41_N (a), Fe_SBA15 (b) and Katalco$_{JM}$ 32-5 (c).

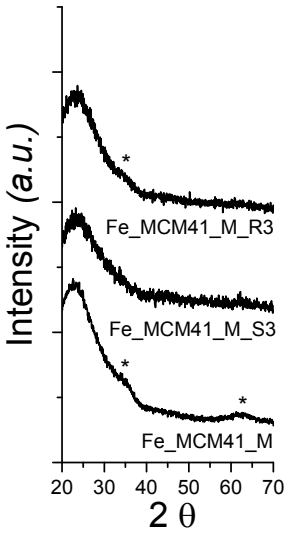


**Figure 4S:** Wide angle XRD patterns of fresh (Fe_MCM41_M), sulphidated (Fe_MCM41_M_S3) and regenerated **(**FeMCM41_M_R3) Fe_MCM41_M.

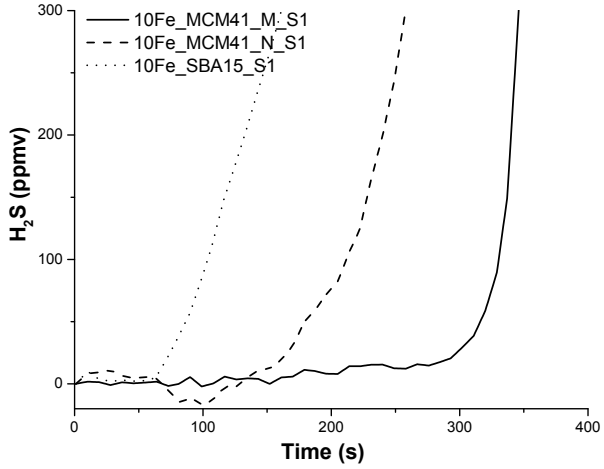


**Figure 5S:** $H_2S$ breakthrough curves of the first sulphidation for the samples Fe_MCM41_M_1S, Fe_MCM41_N_1S and 10Fe_SBA15_1S.

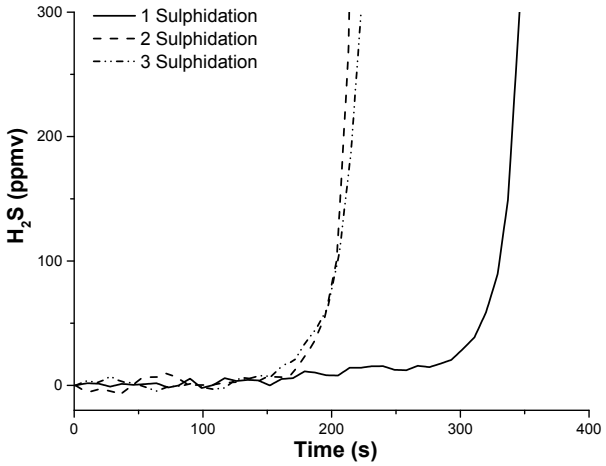


(a)

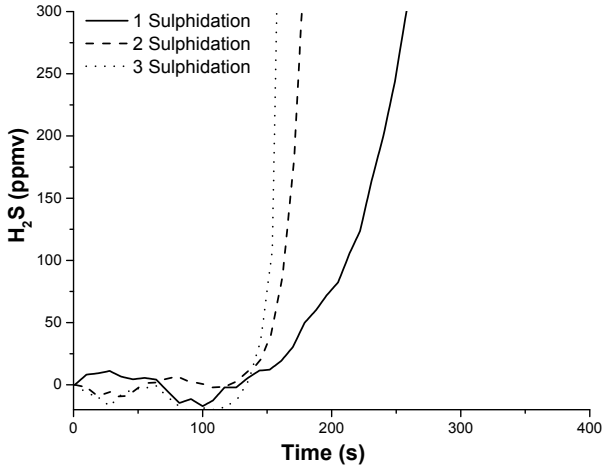


(b)

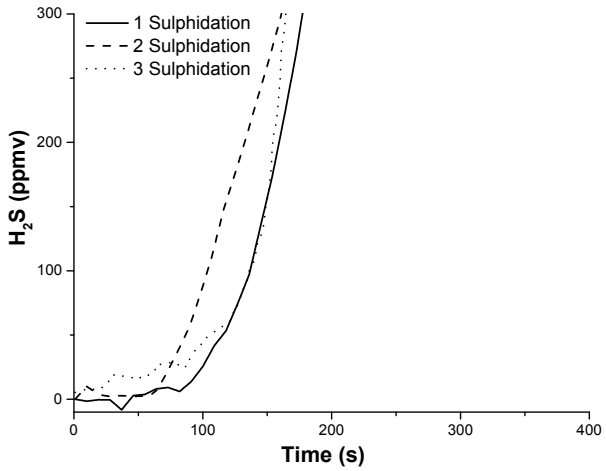


(c)

**Figure 6S:** $H_2S$ breakthrough curves upon three sulphidation–regeneration cycles for the sample Fe_MCM41_M (a), Fe_MCM41_N (b) and Fe_SBA15 (c).